2013

Carbon nanotube-reduced graphene oxide composites for thermal energy harvesting applications

Mark S. Romano
University of Wollongong, mromano@uow.edu.au

Na Li
Nankai University

Dennis Antiohos
University of Wollongong, dennisa@uow.edu.au

Joselito M. Razal
University of Wollongong, jrazal@uow.edu.au

Andrew Nattestad
University of Wollongong, anattest@uow.edu.au

See next page for additional authors

Carbon nanotube-reduced graphene oxide composites for thermal energy harvesting applications

Abstract

By controlling the SWNT-rGO electrode composition and thickness to attain the appropriate porosity and tortuosity, the electroactive surface area is maximized while rapid diffusion of the electrolyte through the electrode is maintained. This leads to an increase in exchange current density between the electrode and electrolyte which results in enhanced thermocell performance.

Keywords

composites, oxide, graphene, applications, reduced, nanotube, carbon, harvesting, energy, thermal

Publication Details

Romano, M. S., Li, N., Antiohos, D., Razal, J. M., Nattestad, A., Beirne, S., Fang, S., Chen, Y., Jalili, R., Wallace, G. G., Baughman, R. & Chen, J. (2013). Carbon nanotube-reduced graphene oxide composites for thermal energy harvesting applications. Advanced Materials, 25 (45), 6602-6606.

Authors

Mark S. Romano, Na Li, Dennis Antiohos, Joselito M. Razal, Andrew Nattestad, Stephen Beirne, Shaoli Fang, Yongsheng Chen, Rouhollah Jalili, Gordon G. Wallace, Ray Baughman, and Jun Chen

DOI: 10.1002/adma.201301754
Article type: Communication

Carbon Nanotube - Reduced Graphene Oxide Composites for Thermal Energy Harvesting Applications

Mark S. Romano, Na Li, Dennis Antiohos, Joselito M. Razal, Andrew Nattestad, Stephen Beirne, Shaoli Fang, Yongsheng Chen, Rouhollah Jalili, Gordon G. Wallace, Ray Baughman,* and *Jun Chen**

M. S. Romano, D. Antiohos, Dr. J. M.Razal, Dr. A. Nattestad, Dr. S. Beirne, R. Jalili, Prof. G. G. Wallace, Associate Prof. J. Chen
Intelligent Polymer Research Institute, ARC Centre of Excellence for Electromaterials Science, Australian Institute of Innovative Materials, Innovation Campus, University of Wollongong, Northfields Avenue, Wollongong, NSW 2522 Australia
E-mail: junc@uow.edu.au, gwallace@uow.edu.au
Dr. S. Fang, Prof. R. Baughman
Alan G. MacDiarmid NanoTech Institute, University of Texas at Dallas, Richardson, Texas 75080, USA
N. Li, Prof. Y. Chen
Institute of Polymer Chemistry, College of Chemistry, Nankai University, Tianjin 300071, China

Keywords: Reduced graphene oxide; carbon nanotubes; thermogalvanic cells, thermocells

One possible solution to the world's growing energy problem is to improve the efficiency of energy conversion processes by harnessing their waste heat.[1] At present, 70 % of the energy generated in cars is dissipated into the environment through hot exhaust pipes and brakes. Even the most efficient internal combustion engines only operate at ~50 % efficiency, with the remainder ending up as waste heat.[2] A popular method by which conversion of thermal to electrical energy can be achieved is through solid-state thermoelectrics. However, due to the high cost and inflexible nature of thermoelectric devices their applications have been limited.[3]

Thermogalvanic systems, also known as thermocells, are simple devices that allow direct transduction of thermal to electrical energy. The recent development of a flexible thermocell allows this system to be employed on curved surfaces wherein waste heat may be sourced, such as automobile exhaust pipes or cooling/heating pipes in factories and power plants.[4] A schematic diagram of the thermocell used in this study is shown in **Figure 1**. This

device consists of two electrodes, immersed in an aqueous solution of ferri/ferro cyanide, that are exposed to different temperatures. The thermal gradient causes a difference in the redox potential of the electrolyte at the electrodes, thus allowing power generation.[5] Electrons extracted at the anode by oxidation of $Fe(CN)_6^{4-} \rightarrow Fe(CN)_6^{3-}$ travel through an external circuit to be consumed at the cathode via reduction of $Fe(CN)_6^{3-} \rightarrow Fe(CN)_6^{4-}$. This electrochemical pathway that thermocells utilize to attain energy conversion allows continuous operation without any moving parts.[6] Convection and diffusion in the cell prevent excessive build-up of reaction products at either half-cell thus facilitating long term stability.[7]

Initial research on thermocells focused on platinum electrodes, the archetypal non-reactive catalytic material.[7-9] In order to make thermocells commercially viable, the electrode material needs to be replaced such that the price per Watt is minimized and an efficiency between 2-5 %, relative to a Carnot engine, is attained.[9] Carbon nanotubes (CNTs) and reduced graphene oxide (rGO) are ideal candidates for thermocell electrodes as they exhibit fast electron transfer kinetics and Nernstian behavior with the ferri/ferro cyanide redox couple.[10] Said redox couple is often employed in thermocell applications because of the large voltage that can be induced upon exposure to a thermal gradient.[9, 11] Individually, CNTs and rGO yield promising results in thermocells owing to the porous nature of the resulting electrodes, more so in CNTs than rGO.[4, 12] Porous materials are desirable as they have a larger active area as opposed to flat electrodes, allowing the possibility of a higher exchange current density between the electrode and electrolyte.[13] Thus porous electrodes facilitate the generation of larger net current densities than flat materials.[14] However, ion accessibility must also be considered. To ensure continuous generation of power in a thermocell, reaction products formed at one half-cell must be transported to the opposite side. If either electrode is not supplied with the redox species needed for electron generation or consumption then power production will diminish. This mass transport problem is exacerbated in pure CNT and rGO electrodes owing to the tortuous nature of the former and sheet restacking in the latter.[14] In

this study we aim to enhance the porosity of the thermocell electrode through the use of CNTs, more specifically single walled nanotubes (SWNT), and rGO composites produced from a dispersion in 1-cyclohexyl-2-pyrrolidone (CHP). CHP was selected as only mild sonication conditions are necessary in order to facilitate SWNT exfoliation thus reducing the damage to the tubes by cutting.[15] We show that by controlling the composition and thickness of the SWNT-rGO electrode, we are able to tailor the porosity for thermocell applications. The areal power density (P_{area}) or mass power density (P_{mass}) is normalized to the temperature gradient (ΔT^2) to take into account the difference in ΔT of thermocells run at different operating temperatures.[4] By using our optimized SWNT-rGO electrode in a novel stacked electrode configuration, we attain a $P_{area}/\Delta T^2$ that is ~380 % higher and $P_{mass}/\Delta T^2$ that is ~280 % larger than previously achieved using SWNT-rGO composite electrodes.[14] More importantly, the thermocell efficiency we achieved is 2.63 % relative to a Carnot engine, almost double the highest reported value and within the range for commercial viability of these devices.[4, 9]

1 µm thick electrodes of pure SWNT, pure rGO and SWNT:rGO composites (95:5, 90:10, and 80:20 weight ratio) were investigated to determine the optimum composition for thermocells (electrode preparation details can be found in experimental and **Figure S1**). The addition of rGO to SWNT does not affect the quality of the SWNT dispersion as evidenced by the peaks that appear in the low frequency of the Raman spectra (**Figure S2**). Said peaks (~219.74 cm^{-1}, ~258.41 cm^{-1}, and ~284.20 cm^{-1}) correspond to the radial breathing mode and arise due to the vibration of carbon atoms along the SWNT tube/bundle diameter.[16] As there is very little variation in peak position, it may be inferred that bundle diameter is the same across the different compositions of SWNT-rGO samples (**Table S1**). Measurement of the defects in the rGO structure may be done by comparing the D (~1350 cm^{-1}) - to - G (~1600 cm^{-1}) band intensity ratio (I_D/I_G).[17] The D band is indicative of defects that may be may be associated with the edges of the sheet or defects on the basal plane and is linked with the degree of disorder of the sample.[18] Raman spectra of the rGO sample reveal that rGO has

I_D/I_G = 1.316. This value indicates that the sample has structural imperfections that may be attributed to topological defects (introduced during thermal reduction) and residual oxygen containing functional groups (introduced during the oxidation step of rGO synthesis) that act as defects on the basal plane and edges of the rGO sheets.[19] Raman spectra of the SWNT-rGO composites are similar to that of pure SWNT as the composites used were predominantly composed of SWNTs. It is worth noting that comparison of I_D/I_G (Table S1) indicates a slight increase in the ratio (from 0.104 for pure SWNT to 0.155 for 80% SWNT) as the amounts of rGO added to the sample is increased. The rise in I_D/I_G is caused by the increase in defective sites associated with the rGO sheets.

The cross section of the vacuum filtered SWNT film (**Figure 2a**) depicts a uniform, dense mat of tubes. Figure 2b shows that the gaps are generated at the SWNT-rGO interface; i.e. gaps are generated between SWNT mats, presumably due to the presence of rGO sheets. The enhanced porosity of the SWNT-rGO composite as compared to pure SWNT films may improve electrolyte diffusion and increase catalytic surface area.

This last point is confirmed with cyclic voltammetry (CV), as the peak current density gives insight to the electroactive surface area (ESA).[20] Cyclic voltammograms shown in **Figure S3** clearly indicate an increase in faradaic peak current for the various carbon materials as compared to platinum. Also, the SWNT-rGO composites have larger faradaic peak currents compared to SWNT and rGO individually. Since all the electrodes used exhibit reversible kinetics, the rise in faradaic peak current can be attributed to increased ESA when the two different carbon materials are combined, as given by Equation 1.[21]

$$I_{p-f} \propto \sqrt{Dv} C_o A \quad (1)$$

Where I_{p-f} is the faradaic peak current, D the diffusion coefficient, v the scan rate, C_o the initial concentration, and A the ESA. The largest ESA (**Figure S4**) was obtained using the 90 % SWNT-10 % rGO composite (henceforth referred to as 90-10). At a 10 mV s^{-1} scan rate, the peak separation for the various carbon materials are similar to that of platinum; indicating

that the carbon electrodes drive the electron transfer reaction at roughly the same rate as that of platinum.

In general, CV run at low potential scan rates approximate electrochemical equilibrium at electrode surfaces. When the scan rate is increased the rate of electron transfer may become competitive with the potential sweep rate. Under these conditions, the potential difference between the oxidation and reduction peak may provide qualitative insight to the kinetics of the electron transfer process.[22] Sluggish electrode kinetics translates to greater potential or time to deplete all the ions at the electrode surface resulting in larger peak separations. CV run at 200 mV s^{-1} (Figure 2c) shows that the peak separation of the 90-10 (this composite was selected as it resulted in the largest peak currents) versus that of SWNT and rGO is smaller, implying that the composite possesses the fastest electron transfer kinetics. The tortuous nature of the SWNT film hinders the flow of ions through the electrode which accounts for its much more sluggish kinetics. This is reflected in the Nyquist plot (**Figure S5**), which shows that the charge transfer resistance ($R_{ct,}$ diameter of the semicircle[23]) is larger for the SWNT film as compared to the 90-10. The slower kinetics of the rGO film may be attributed to the defects introduced during synthesis; evidenced by the D-band in the Raman spectra (Figure S2) and the larger series resistance (the intercept of the left side of the curve with the x-axis of the Nyquist plot[24] in Figure S5) as compared to the 90-10. Defects act as electron scattering sites thereby decreasing conductivity.[25]

Thermocell testing (Figure 2d and 2e) reveals both rGO and SWNT achieve P_{area} ~30% higher than platinum. This increase can be attributed to the larger ESA of the carbon materials as evidenced by their morphology and cyclic voltammograms. More importantly, by controlling the amounts of SWNT and rGO, thermocell performance is further enhanced. The 90-10 composite showed the best performance, generating 0.327 W m^{-2} at ΔT = 31 ^{o}C. The higher P_{area} generated through the use of the 90-10 may be attributed to its fastest kinetics (Figure 2c) and largest ESA (Figure S4) among all carbon electrode compositions tested. A

greater amount of rGO may lead to restacking of the sheets due to van der Waals interactions thus reducing the ESA.[26] On the other hand, having less than 10 wt % rGO results in a structure that is more tortuous as evidenced by the larger R_{ct} of the pure SWNT film (Figure S5). A greater degree of tortuosity impedes ion movement through the electrode resulting in lower thermocell performance.[14]

In order to improve thermocell performance it is desirable to further increase the exchange current density between the electrode and electrolyte; as this yields a larger net current density. An obvious approach to achieving this is to increase the electrode thickness of the 90-10 (1.0, 1.5, 2.5, 4.5, 6.6 and 10.5 μm) to facilitate an increase in electroactive sites. Surface images (**Figure S6**) of the 90-10 show the typical SWNT-rGO interface wherein a more "open" structure surrounding the rGO sheets can be seen. Selected cross-sectional images, **Figure 3a and b** (detailed comparison is shown in **Figure S7**), depict similar morphologies where the interaction of SWNT and rGO generates a layered and "open" cross section. The Nyquist plot (**Figure S8**) indicates that R_{ct} scales with film thickness. R_{ct} for the 1.0 μm is indistinguishable whereas it is 27.5 and 34.8 Ω for the 4.5 and 10.5 μm films respectively. The degree of tortuosity of the films is directly proportional to its thickness owing to the random nature of the pores. We believe that this increased tortuosity restricts ion accessibility resulting in larger R_{ct}. Cyclic voltammograms (**Figure 3c**) indicate that the ESA plateaus beyond a thickness of 4.5 μm. These findings are consistent with thermocell testing (Figure 3d and e) with P_{area} up to 0.46 W m^{-2}. The film density (Figure 3e) increases initially then tapers off at the 4.5 μm film. This trend may provide insight as to how the film porosity changes with increasing thickness; i.e. the balance between porosity and film thickness is attained at the 4.5 μm film. For continuous power output in thermocells, reactants at the cathode need to be replenished by the reaction products formed at the anode and vice versa.[7] Electrodes must be structured so as to facilitate this diffusion process and thus minimize the mass transport resistance. Extended tests of the 4.5 μm film (**Figure S9**) indicate a stable

power output over a period of 48 hours, suggesting that detrimental build-up of concentration gradients in the thermocell doesn't occur. As film thickness is increased, the random orientations of the pores leads to increased tortuosity of the film thus exacerbating the problems associated with reactant/product diffusion, especially through the electrode; i.e. thicker materials have longer diffusion paths. Films thicker than 4.5 μm will only lead to a waste of material as not all sites may be accessed by the electrolyte thus will not participate in the redox processes required for thermal harvesting.

Using the optimized electrode, we employ a stacked electrode configuration (Figure 3f) to take further advantage of the ESA of the SWNT-rGO film. Stainless steel mesh placed between the stacked SWNT-rGO films provides electrical conductivity and also facilitates ionic diffusion between stacked electrodes. Preliminary tests involving ten stacked films (per side) yield a four-fold increase in P_{area} (1.85 W m^{-2}) than that of a single electrode (non-stacked) configuration (0.46 W m^{-2}, Figure 3g). Previous work using SWNT-rGO composite electrodes yield $P_{area}/\Delta T^2$ of 0.4 mW m^{-2} K^{-2} and $P_{mass}/\Delta T^2$ of 13 mW kg^{-1} K^{-2}.[14] We attain ~380 % and ~280 % improvements in $P_{area}/\Delta T^2$ (1.9 mW m^{-2} K^{-2}) and $P_{mass}/\Delta T^2$ (49 mW kg^{-1} K^{-2}), respectively. These results demonstrate enhanced thermocell performance using significantly less active material. These developments imply a lower price per Watt, thus making thermocells more cost effective to produce. More importantly, the combination of the optimized electrode composition, thickness, and the new stacked electrode configuration resulted in efficiency of 2.63 % relative to a Carnot engine (Φ_r, Figure S10). This Φ_r is a remarkable 88 % improvement compared to the highest reported Φ_r in thermocells (1.4 %).[4]

In conclusion, by optimizing electrode composition and thickness, we have attained a delicate balance between porosity and tortuosity that favors rapid electrolyte diffusion and more efficient access of the electroactive surface area of the electrode. Using the optimized SWNT-rGO electrode in a novel stacked electrode configuration achieved a record thermocell

performance that is already within the range for commercial viability (i.e. Φ_r between 2 to 5 %).[9]

Experimental

SWNT-rGO synthesis and characterization: Figure S1 outlines the process used to prepare the carbon films used. Briefly, SWNTs (HiPco, Continental Carbon Nanotechnologies Inc.) were dispersed using CHP at a concentration of 1 mg ml^{-1} using a combination of bath (Branson B1500R-MT) and probe sonication (Branson probe sonifier). The dispersion was left overnight for reaggregation to occur after which it was centrifuged (Eppendorf Centrifuge 5415 D) for 90 minutes at 2500 rcf. The concentration of the supernatant was determined via Ultra Violet-Visible Spectroscopy (Shimadzu UV-1800) then diluted to 0.4 mg ml^{-1}.

Graphene oxide (GO) was synthesized using a modified Hummers method developed by Marcano et al [27]. The dried GO was exfoliated using a commercial 1200 W microwave. The resulting powder was dispersed in CHP following the procedure on SWNT dispersion.

For electrode composition optimization, films with a thickness (VeecoDektak 150) of 1 µm and compositions of 100-0, 95-5, 90-10, and 80-20, 0-100 weight percent SWNT-rGO were made. This was done by mixing dispersions of SWNT and rGO via bath sonication for 90 minutes followed by vacuum filtration on Millipore PVDF membrane with a pore size of 0.1 µm. Electrodes were then prepared with a geometric area of 0.785 cm^2. Films of thickness 1.0, 1.5, 2.5, 4.5, 6.5, and 10.5 µm were fabricated using 90-10 after it was shown to be the best ratio. All films were plasma treated in air for 20 minutes to ensure wetting of the electrode (**Figure S11**).

The structure of the electrodes was probed using Raman JY HR800. Sample morphology was investigated using a JEOL JSM-7500FA Field Emission Scanning Electron Microscope Cyclic voltammetry and electrochemical impedance spectroscopy (EIS) were completed using an EDAQ Potentiostat e-corder 401 and Gamry Instruments V.5.58 respectively. Three electrode tests were run at 20 ^oC with a Ag/AgCl reference electrode and platinum mesh

counter electrode. EIS was measured in the frequency range of 100 kHz-10 mHz with an AC amplitude of 10 mV (rms). Both CV and EIS were run using 0.01 M $K_3Fe(CN)_6$ with 0.1 M $NaNO_3$ as the supporting electrolyte in aqueous media in order to reduce the ohmic overpotential in the cell.

Thermocell testing: Thermocell testing was done using a T-Cell (Figure 1) at ΔT~31 ^oC with an electrode separation of 2 cm. One half of the cell was cooled using circulating coolant and the other half was heated using an Omegalux Rope Heater (accuracy ± 1 ^oC) connected to a TCA Control Box. The electrolyte used in all thermocell tests was 0.4 M $K_3Fe(CN)_6/K_4Fe(CN)_6$ in aqueous media. This concentration was selected as it has the ideal combination of thermal and electrical conductivity for thermocells; i.e. low thermal and high electrical conductivity [12]. J-V curves were measured using a Keithley 2400 sourcemeter and customized LabView software.

Acknowledgements
The authors gratefully acknowledge funding from the Department of Science and Technology, Philippines and the Australian Research Council Centre of Excellence for Electromaterials Science. They acknowledge the UOW Electron Microscopy Centre and Australian National Fabrication Facility for provision of services and equipment access. Financial support for UTD authors was from Air Force grant FA9550-11-C-0061.

Supporting Information is available online from Wiley InterScience or from the author.

Received: ((will be filled in by the editorial staff))
Revised: ((will be filled in by the editorial staff))
Published online: ((will be filled in by the editorial staff))

References

[1] a) P. J. Hall, E. J. Bain, *Energy Policy* **2008**, *36*, 4352; b) A. K. Shukla, S. Sampath, K. Vijayamohanan, *Curr. Sci.* **2000**, *79*, 6; c) P. J. Hall, M. Mirzaeian, S. I. Fletcher, F. B. Sillars, A. J. R. Rennie, G. O. Shitta-Bey, G. Wilson, A. Cruden, R. Carter, *Energy Environ. Sci.* **2010**, *3*, 1238.

[2] Wartsila, http://www.wartsila.com/en/engines/low-speed-engines/RT-flex96C, **2012**.

[3] C. B. Vining, *Nat. Mater.* **2009**, *8*, 83.

[4] R. Hu, B. A. Cola, N. Haram, J. N. Barisci, S. Lee, S. Stoughton, G. Wallace, C. Too, M. Thomas, A. Gestos, M. E. d. Cruz, J. P. Ferraris, A. A. Zakhidov, R. H. Baughman, *Nano Lett.* **2010**, *10*, 838.

[5] H. G. Hertz, S. K. Ratkje, *J. Electrochem. Soc.* **1989**, *136*, 1698.

[6] Y. V. Kuzminskii, V. A. Zasukha, G. Y. Kuzminskaya, *J. Power Sources* **1994**, *52*, 231.

[7] T. I. Quickenden, Y. Mua, *J. Electrochem. Soc.* **1995**, *142*, 3652.

[8] Y. Mua, T. I. Quickenden, *J. Electrochem. Soc.***1996**, *143*, 2558.

[9] T. I. Quickenden, Y. Mua, *J. Electrochem. Soc.* **1995**, *142*, 3985.

[10] a) J. M. Nugent, K. S. V. Santhanam, A. Rubio, P. M. Ajayan, *Nano Lett.* **2001**, *1*, 87; b) M. F. El-Kady, V. Strong, S. Dubin, R. B. Kaner, *Science* **2012**, *335*, 1326; c) L. Tang, Y. Wang, Y. Li, H. Feng, J. Lu, J. Li, *Adv. Funct. Mater.* **2009**, *19*, 2782.

[11] T. I. Quickenden, C. F. Vernon, *Sol. Energy* **1986**, *36*, 63.

[12] M. Romano, S. Gambhir, J. Razal, A. Gestos, G. Wallace, J. Chen, *J. Therm. Anal. Calorim.* **2012**, *109*, 1229.

[13] Z. Qian, Y. Shaojun, Z. Jing, Z. Ling, K. Pingli, L. Jinghong, X. Jingwei, Z. Hua, S. Xi-Ming, *Nanotechnology* **2011**, *22*, 494010.

[14] T. J. Kang, S. Fang, M. E. Kozlov, C. S. Haines, N. Li, Y. H. Kim, Y. Chen, R. H. Baughman, *Adv. Funct. Mater.* **2012**, *22*, 477.

[15] S. D. Bergin, V. Nicolosi, P. V. Streich, S. Giordani, Z. Sun, A. H. Windle, P. Ryan, N. P. P. Niraj, Z.-T. T. Wang, L. Carpenter, W. J. Blau, J. J. Boland, J. P. Hamilton, J. N. Coleman, *Adv. Mater.* **2008**, *20*, 1876.

[16] a) C. G. Salzmann, S. A. Llewellyn, G. Tobias, M. A. H. Ward, Y. Huh, M. L. H. Green, *Adv. Mater.* **2007**, *19*, 883; b) M. S. Dresselhaus, G. Dresselhaus, R. Saito, A. Jorio, *Phys. Rep.* **2005**, *409*, 47.

[17] U. Khan, A. O'Neill, M. Lotya, S. De, J. N. Coleman, *Small* **2010**, *6*, 864.

[18] C. Casiraghi, A. Hartschuh, H. Qian, S. Piscanec, C. Georgi, A. Fasoli, K. S. Novoselov, D. M. Basko, A. C. Ferrari, *Nano Lett.* **2009**, *9*, 1433.

[19] H. C. Schniepp, J.-L. Li, M. J. McAllister, H. Sai, M. Herrera-Alonso, D. H. Adamson, R. K. Prud'homme, R. Car, D. A. Saville, I. A. Aksay, *J. Phys. Chem. B* **2006**, *110*, 8535.

[20] M. Pacios, M. del Valle, J. Bartroli, M. J. Esplandiu, *J. Electroanal. Chem.* **2008**, *619-620*, 117.

[21] A. J. Bard, L. R. Faulkner, *Electrochamical Methods-Fundamentals and Applications,* John Wiley and Sons, Inc, NY, USA **2001**.

[22] R. S. Nicholson, *Anal. Chem.* **1965**, *37*, 1351.

[23] J. E. B. Randles, *Discuss. Faraday Soc.* **1947**, *1*, 11.

[24] S.-M. Park, J.-S. Yoo, *Anal. Chem.* **2003**, *75*, 455 A.

[25] S. Park, D. A. Dikin, S. T. Nguyen, R. S. Ruoff, *J. Phys. Chem. C* **2009**, *113*, 15801.

[26] H. Chen, M. B. Müller, K. J. Gilmore, G. G. Wallace, D. Li, *Adv. Mater.* **2008**, *20*, 3557.

[27] D. C. Marcano, D. V. Kosynkin, J. M. Berlin, A. Sinitskii, Z. Sun, A. Slesarev, L. B. Alemany, W. Lu, J. M. Tour, *ACS Nano* **2010**, *4*, 4806.

[28] S. H. Shiau, C. W. Liu, C. Gau, B. T. Dai, *Nanotechnology* **2008**, *19*, 105303.

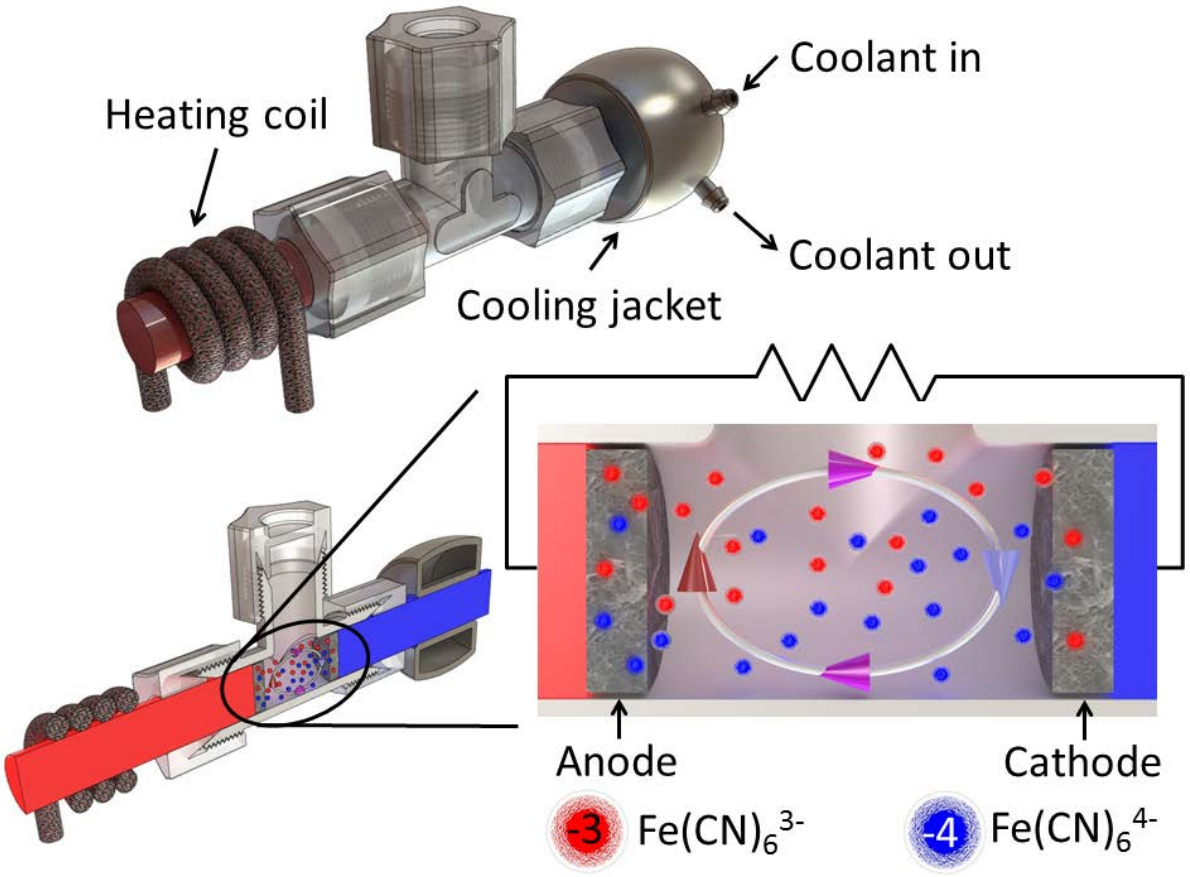

Figure 1. Schematic of a thermocell using the ferri/ferrocyanide redox couple.

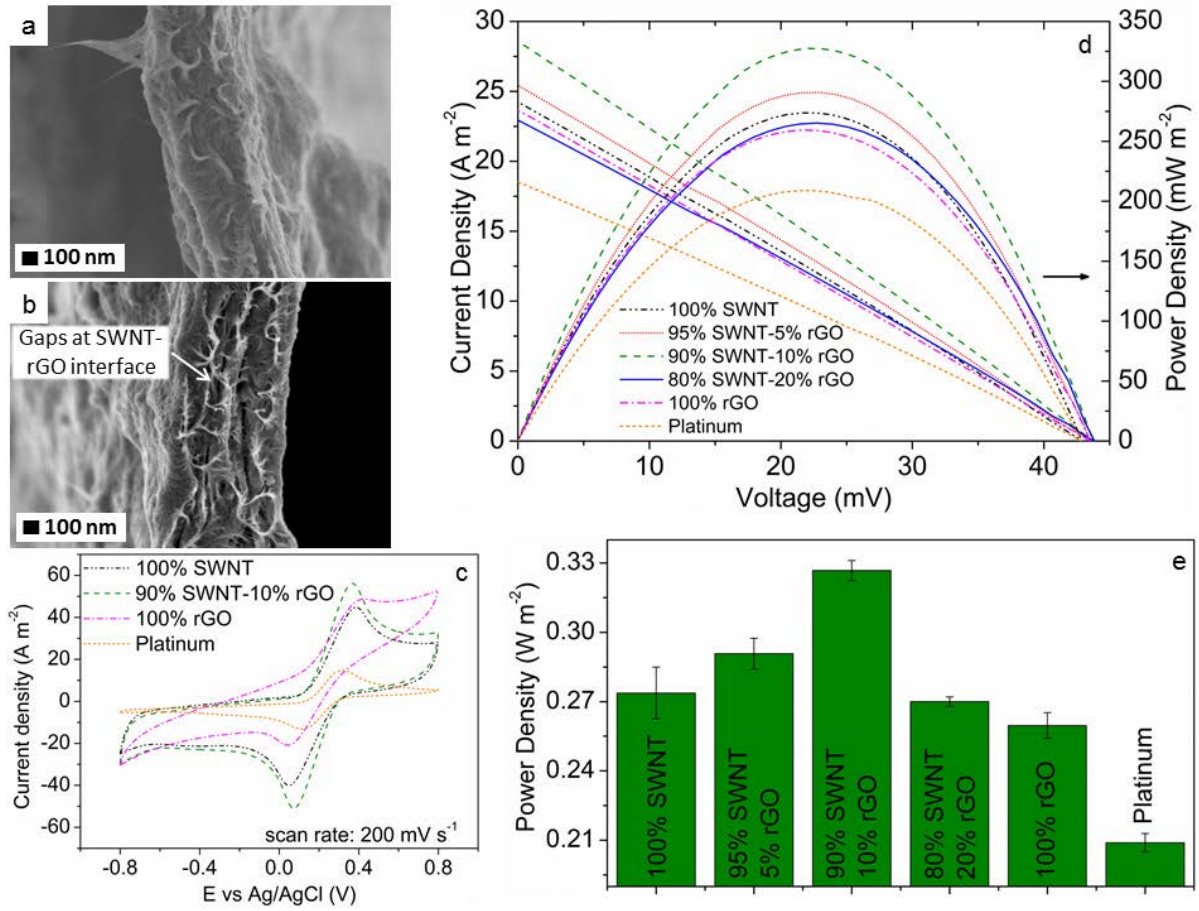

Figure 2. Micrographs of films of a) SWNT, b) 90 % SWNT-10 % rGO composite cross-section. c) Cyclic voltammograms obtained at 200 mV s^{-1} using various electrode materials. d) J-V and P-V curves, e) power density generated using various electrode compositions at ΔT = 31 ^{o}C.

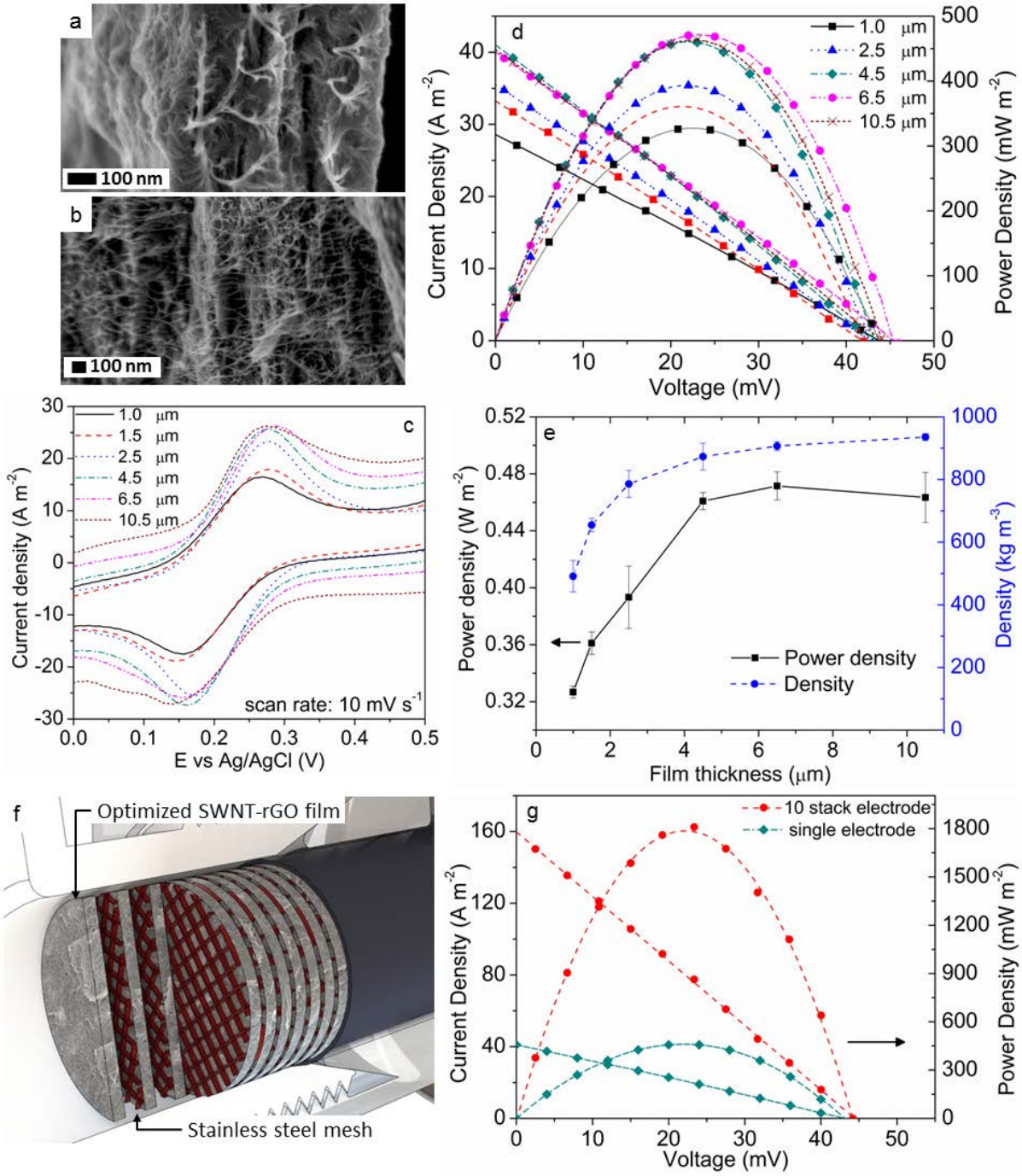

Figure 3. Cross-sectional micrographs of a) 1.0μm, b) 4.5 μm thick films of 90 % SWNT-10 % rGO composite. c) Zoomed in cyclic voltammograms obtained at 10 mV s^{-1}, d) J-V and P-V curves, and e) power density and density of 90 % SWNT – 10 % rGO electrodes of increasing thickness. f) Schematic of the stacked electrode configuration. g) J-V and P-V curves obtained using various electrode configurations. ΔT = 31 ^{o}C

The table of contents entry

By controlling the SWNT-rGO electrode composition and thickness so as to attain the appropriate porosity and tortuosity, the electroactive surface area is maximized while rapid diffusion of the electrolyte through the electrode is maintained. This leads to an increase in exchange current density between the electrode and electrolyte which results in enhanced thermocell performance.

Keyword: Reduced graphene oxide; carbon nanotubes; thermogalvanic cells, thermocells

M.S. Romano, N. Li, D. Antiohos, J.M. Razal, A. Nattestad, S. Beirne, S. Fang, Y. Chen, R. Jalili, G.G. Wallace*, R. Baughman, J. Chen*

Carbon Nanotube - Reduced Graphene Oxide Composites for Thermal Energy Converters